Strain Dependent Local Phase Transitions Observed during Controlled Supercontraction Reveal Mechanisms in Spider Silk

Philip T. Eles† and Carl A. Michal*

Department of Physics and Astronomy, University of British Columbia, 6224 Agricultural Rd, Vancouver, B.C., Canada V6T 1Z1

Received October 16, 2003; Revised Manuscript Received December 12, 2003

ABSTRACT: Spider dragline silk is a semicrystalline protein polymer in which alanine-rich crystalline regions are connected by soft glycine-rich linkers that, in dry fibers are quiescent but become motionally active when plasticized by water. Using solid-state NMR to probe molecular motion and orientation of selectively ^{13}C-labeled glycine residues, we observe a collapse of amino acid chains in hydration-induced local phase transitions and find that the relative abundance of the static and mobile phases can be controlled by fiber strain. Our results suggest a molecular mechanism for silk's mechanical properties based on latent entropic springs that are drawn in preformed extended structures, stabilized by interchain hydrogen bonding, and collapsed by hydration.

1. Introduction

Spider silks are protein fibers whose mechanical properties range from strong and stiff to soft and elastic[1] depending on species, silk gland, and environmental conditions. Silks have become the subjects of intensive study,[2,3] in part due to advances in recombinant DNA technology,[4] which promises to allow large-scale production of silk-inspired fibers having properties customized by amino acid sequence[5,6] and spinning conditions.[7] Realization of this promise depends on a thorough understanding of the microscopic structural basis of the fibers' macroscopic properties.[8]

Many polymer fibers, including dragline silks, demonstrate a phenomenon known as supercontraction,[9] where an absorbed solvent induces large-scale molecular motions in a transition from a glassy to a rubbery state, causing a macroscopic reduction in the length of the fiber and a concomitant swelling in diameter. Supercontraction in synthetic polymers is usually observed only at high temperature or in harsh solvents, whereas spider silks supercontract in water at room temperature.[9,10] It has been suggested that in nature, supercontraction induced by morning condensation maintains tension in spider webs.[9] On the basis of measurements of diminishing supercontraction stress as a function of time, this suggestion was later challenged[11] but is supported by more recent measurements.[12]

Because of its sensitivity to dynamics, solid-state NMR has been used to probe supercontracted silk.[13−15] Other NMR experiments have probed local structure[16,17] and bulk orientation[17,18] in dry silk. However, due to the challenges of uniformly varying strain in large oriented fiber bundles, molecular orientation and dynamics in partially supercontracted samples have not previously been studied.

We employ a two-dimensional (2D) solid-state NMR technique known as DECODER (direction exchange with correlation for orientation distribution evaluation and reconstruction)[19] that, for oriented samples, facilitates a full reconstruction of the orientation distribution of static molecular subunits within a polymer by correlating the chemical shift frequencies of nuclear spins at two macroscopic sample orientations. Our sample geometry, fibers wrapped around a collapsible plastic support whose axis lies parallel to the NMR coil axis, complicates the orientation distribution reconstruction but allows control of the sample strain and environmental conditions.[18]

In addition to orientation, the DECODER experiment is sensitive to molecular motions on a number of time scales (see Figure 1). Motions with correlation times, τ_c, less than 1/(10 Hz) cause a loss of correlation during the mixing time of the experiment (100 ms) and result in a 2D spectrum that is simply the product of the one-dimensional spectrum with itself. Motions faster than ∼20 kHz average the ^{13}C chemical shift anisotropy, reducing the wide-line spectrum into a sharp peak at the isotropic chemical shift, and also average the ^{1}H−^{13}C dipolar couplings resulting, for cross-polarization experiments like ours, in a loss of signal intensity. Still faster motions manifest themselves in enhanced spin relaxation, to which this experiment is relatively insensitive because the mixing and evolution times are much shorter than the fastest T_1 in any of our silk samples.

In this work, we restrain silk fiber bundles before hydration, allowing them to supercontract to varying predetermined lengths, and measure protein backbone orientation and dynamics as a function of degree of supercontraction. In such a way, we obtain snapshots of silk in the process of supercontraction.

2. Experimental Section

Silk Samples. The NMR experiments were carried out on 1-^{13}C-glycine-labeled silk samples under three different conditions of restraint: the first was used as collected and was under considerable draw tension, estimated at 50% of the fibers' breaking strength, corresponding to a strain of about 10%. The second sample was allowed to contract 10% in length, largely relieving the draw tension. Finally, the first sample was cut off the collection spool and rolled into an isotropic bundle and so was not restrained.

Dragline silk from adult female *Nephila clavipes* spiders fed a 1-^{13}C-glycine-enriched diet was spooled at 2 cm/s onto poly(tetrafluoroethylene) (PTFE) rods that had been hollowed, slit on one side, and expanded with poly(chlorotrifluoroethylene)

* To whom correspondence should be addressed. E-mail: michal@physics.ubc.ca.
† E-mail: elespt@physics.ubc.ca.

10.1021/ma035567p CCC: $27.50
Published on Web 01/21/2004

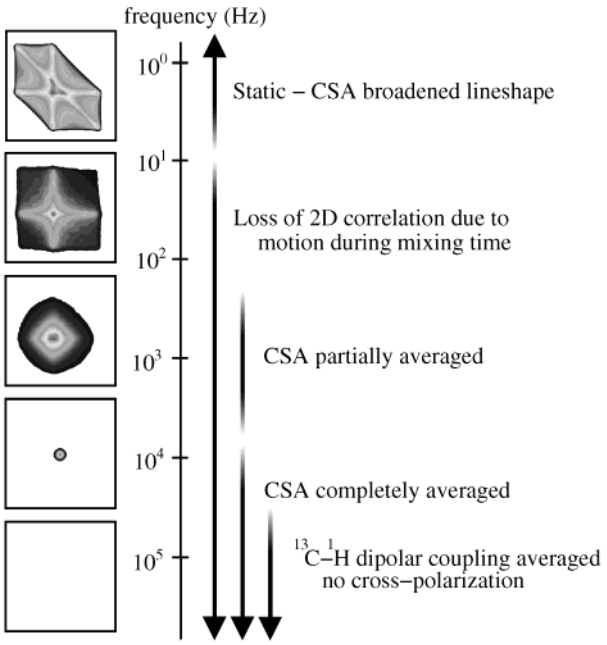

Figure 1. Molecular motions on multiple time scales can be differentiated based on spectral characteristics in the DECODER experiment. Simulated powder spectra are shown in the different motional regimes.

(PCTFE) cylindrical inserts that could be later removed to relax the drawing tension.[18] NMR spectra of restrained samples were obtained with the silk on the collecting rod and hydration was achieved by placing a water-filled NMR tube over the end of the sample and sealing with PTFE tape. Unrestrained spectra were collected from silk that had been removed from the rod and packed unoriented inside a hollowed PCTFE cylinder. Hydration was achieved by filling the sample holder with water before sealing.

NMR Spectroscopy. ^{13}C DECODER NMR spectra were collected at 91.480 MHz on a home-built NMR spectrometer[20] with a home-built doubly tuned wide-line probe equipped to rotate the sample about the solenoidal rf coil axis via a spectrometer-controlled stepper motor. Spectra were collected with 5 μs 90° carbon pulses, a cross-polarization contact time of 1.5 ms, CW proton decoupling at 50 kHz during both evolution periods, and a 90° rotation of the sample about the rf coil axis during the 0.1 s mixing time. Spectra were zero-filled to achieve the same spectral resolution in both dimensions and apodized with a 50 Hz full width at half-maximum (fwhm) exponential before Fourier transformation.

Spectral Reconstruction. The unrestrained carbonyl spectra were decomposed into contributions from static ($1/\tau_c$ < 10 Hz) and mobile ($1/\tau_c$ > 10 kHz) components by fitting a linear superposition of a simulated carbonyl powder spectrum with chemical shift tensor values of [242, 178, 96] ppm,[17] and a sharp (1.9 kHz fwhm) peak at the isotropic chemical shift (172 ppm). The restrained spectra were reconstructed by a linear superposition of subspectra simulated for a discrete set of molecular orientations of the CSA tensor in the silk fiber using the PORT Mathematical Subroutine Library's (AT&T Bell Labs, Murray Hill, NJ) adaptive nonlinear least-squares fitting algorithm.[21] A two-component model, details of which are described elsewhere,[18] was used to decompose the broad carbonyl spectrum into contributions from a well aligned and poorly aligned component in addition to a mobile component identical to that used above.

Mass Spectroscopy. Electrospray mass spectroscopy was performed on a portion of the sample that had been hydrolyzed in HCl for 24 h at 100°. The isotopic analysis indicated that approximately 84% of the signal intensity of the dry sample arises from glycines, with the remainder coming largely from alanines. Thus, no background subtraction was deemed necessary.

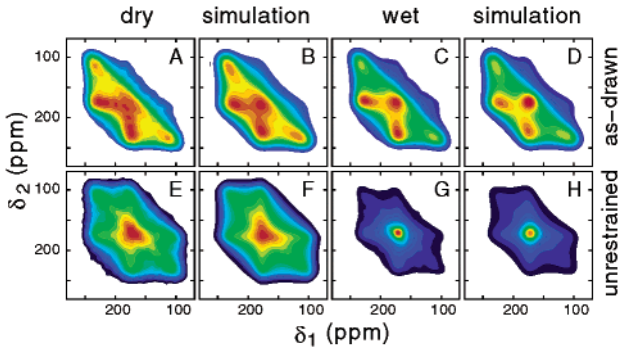

Figure 2. Carbonyl region of ^{13}C DECODER spectra of 1-^{13}C glycine labeled dragline silk. The sample in parts A and C was restrained with drawing tension, unrestrained in parts E and G. Parts B, D, F, and G are simulations described in the text.

3. Results

The ^{13}C DECODER NMR spectra of the silk as-drawn and unrestrained are shown in Figure 2, parts A and E, respectively. The dramatic difference between the as-drawn spectrum and the isotropic powder pattern of the unrestrained spectrum reflects the high degree of orientational order in the silk fibers. The fit shown for the as-drawn spectrum (Figure 2B) is based upon a model[18] incorporating two static components, each of which has an orientation distribution described by a Gaussian centered along the fiber axis.

The fit reveals that one component is well aligned, the other poorly aligned, their distributions having respective fwhm of about 20 and 70° with respect to the fiber axis. The unrestrained spectrum is fit (Figure 2F) solely to an isotropic static powder pattern. It is clear from these spectra, along with one-dimensional ^{13}C NMR spectra acquired without cross-polarization that there is little molecular motion at time scales faster than ~10 Hz.

Spectra for these same samples when hydrated are shown in Figure 2, parts C and G. Upon hydration, a sharp peak appears at the isotropic chemical shift frequency, and the overall spectral intensity decreases. These changes are indicative of large amplitude molecular reorientations on time scales faster than ~20 kHz occurring within some regions of the silk, as the chemical shift anisotropy is well averaged in the sharp peak, and the loss of signal intensity reflects inefficient cross-polarization of the mobile component. In addition to the contribution from the static components, the best fits in Figure 2, parts D and H, include a sharp peak at the isotropic chemical shift to reflect this mobile component.

The DECODER data in Figure 2 completely lack the spectral characteristics of slow motions on the time scale of $10-10^4$ Hz (see Figure 1). This is especially dramatic in the hydrated samples which exhibit both static ($1/\tau_c$ < 10 Hz) and fast moving ($1/\tau_c$ > 10^4 Hz) components but lack an intermediate dynamical regime. The absence of slow motions is also evident from the lack of off-diagonal intensity in a DECODER experiment performed without sample rotation. This is strong evidence that supercontraction is the result of a hydration-induced phase transition between glassy and rubbery states mediated by the disruption of interchain hydrogen bonds by waters of hydration.

The relative abundance of the static and fast components, as determined by the intensities of the multicomponent fits to the data, are summarized in Figure

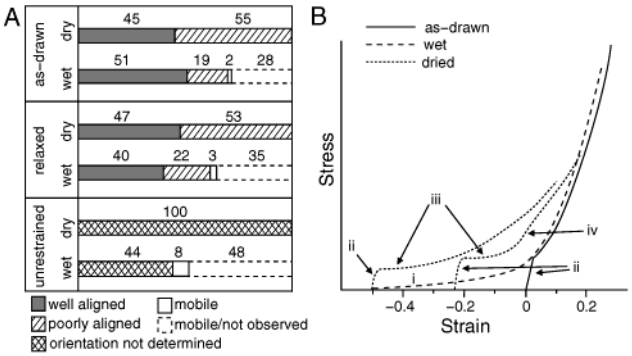

Figure 3. Dependence of orientation, dynamics, and mechanical properties on hydration and strain. (A) Integrated intensity of NMR signals of dry and wet silk fibers under varying strain. The shading of the unrestrained sample reflects the fact that no information on the relative abundance of well and poorly aligned components is obtained. These data suggest a reinterpretation of recently measured stress−strain curves, shown schematically in part B, based on refs 6, 22, and 23 (see text). The dotted curves represent fibers treated by allowing them to partially or fully supercontract before drying.

3A and show a marked increase in the fraction of the sample that becomes mobile as the fiber strain decreases. The degree of orientational order in hydrated silk observed here is in qualitative agreement with X-ray diffraction[24] and birefringence[9] measurements made as a function of strain.

The results of the two-component fits to the restrained samples' spectra indicate that the glycines that become mobile are almost exclusively those that were poorly aligned before hydration. Upon hydration, the remainder of the poorly aligned static fraction is fit by a Gaussian so broad as to be completely isotropic, while the well aligned component retains a fwhm of about 20°. The apparent increase in the population of the well aligned component of the as-drawn sample, from 45 to 51%, upon hydration likely reflects residual alignment of the poorly aligned component, which is now split among the isotropic and well aligned components.

On the basis of the spidroin-1 amino acid sequence,[15] roughly 37% of glycines reside inside or within a few amino acids of the alanine-rich crystalline regions,[14] and are known from previous solid-state NMR[14,26] and X-ray diffraction measurements[24] to remain immobilized upon hydration. The remaining glycines are distributed throughout the intercrystal linkers. The 44% of glycines that we find remain static in the fully supercontracted sample corresponds well with the fraction expected to reside inside or immediately adjacent to the crystalline regions, in agreement with the fraction found by Yang et al.[14] based on the analysis of one-dimensional NMR spectra of fully supercontracted 1-^{13}C-glycine-labeled silk.

On the basis of these orientational and dynamic data, we make a connection between the linker regions, which become mobile during supercontraction, with the poorly aligned component, and the crystalline regions, which are unaffected by hydration, with the well aligned component. These are not rigorous assignments of the fit components, because as mentioned above, there is likely some (strain dependent) contribution from each of the structural regions to each of the fit components, due to the limitations of the two component model in describing the true orientation distribution.

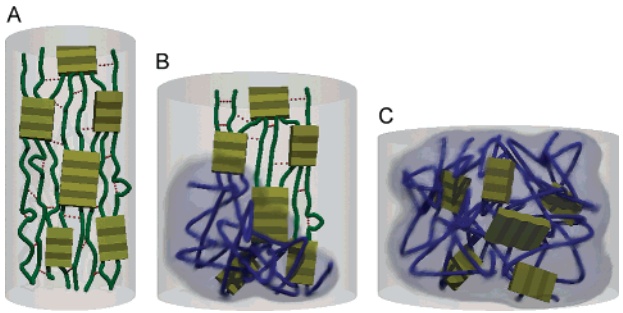

Figure 4. Cartoon depicting the proposed mechanism of fiber supercontraction. (A) Static linkers (green extended chains) in as-drawn dragline silk connect crystalline regions (gold pleated blocks) and are stabilized by interchain hydrogen bonds (red dotted lines). (B) As the hydrated fiber is allowed to contract, an abrupt transition to a highly mobile phase (blue blurred chains) occurs in some regions, increasing local strain and enforcing quiescence in neighboring regions. (C) For a fiber allowed to fully supercontract, more regions become mobile. An actual fiber has a diameter several hundred times that of the region depicted here.

4. Discussion

Our results illuminate the molecular origin of a large body of mechanical and structural measurements (eg. refs 2 and 3 and references therein) for which we propose a model mechanism based on the existence of preformed extended structures in the linker regions of as-drawn silk. The interchain hydrogen bonds stabilizing these structures are broken by fiber stress and hydration; the former leading to elastic and then plastic fiber deformation and the latter leading to local phase transitions to a rubbery state in the process of supercontraction. We outline this model in detail below.

In dry, as-drawn dragline, the linker regions largely assume highly extended conformations[18] (Figure 4A). The amino acid sequence and fiber spinning process encourage the formation of some local structure, possibly extended polyglycine II helices,[16,17] as well as compact turns.[14,27] On hydration, hydrogen bonds stabilizing these structures are broken and the chains collapse into mobile entropic springs, with the fraction of the linker regions able to participate governed by the restrained length of the fiber (Figure 4, parts B and C). On the basis of our results above, the separation between mobile and static components is a sharp one, and is understood in terms of local phase transitions. Existing heterogeneity provides nucleation sites so that regions with low enough local stress cooperatively hydrate and collapse, increasing the stress on neighboring regions, reinforcing their quiescence, as depicted in Figure 4B. The collapse results in a broadening of the orientation distribution of the uncollapsed linkers as the fiber shrinks.

Straining the supercontracted dragline results in a very low initial modulus, as the soft entropic springs extend (region i in Figure 3B). On reaching the extension limits of the springs, chain reorientation and rearrangement dominate the response and the modulus increases.

If allowed to dry while contracted, the entropic spring regions lose their mobility as waters of hydration are replaced with intra- and interchain hydrogen bonds, forming "latent entropic springs", static structures that may regain some local structure,[13] but remain compact. When these fibers are strained, the initial modulus is similar to that of as-drawn dragline (ii of Figure 3B),

which is well accounted for by detailed numerical models[28] that include the rigid crystalline regions in addition to the soft linkers and allow processes such as chain slippage and breakage. As the stress becomes great enough to break hydrogen bonds, there is a pronounced plateau in the stress−strain curve (iii of Figure 3B) as the latent springs elongate.

In the as-drawn dragline, a small, spinning condition dependent fraction of the linker regions exist as latent entropic springs, accounting for the plateau observed in stress−strain curves (iv in Figure 3B). The hysteresis observed in dry fibers[23] is due to the fact that once stretched out, the latent entropic springs contract much more reluctantly than when hydrated, but remain entropically driven. In the absence of water, the contraction is unlikely to complete, as hydrogen bonds, some transient, may reform to stabilize intermediate configurations. Differences between successive load−unload cycles may also be due to the rupturing of the initial extended structures found in as-drawn fibers.

Our proposed model succeeds in explaining the mechanical properties of dragline silk including recent tensile measurements on silk fibers having undergone controlled supercontraction during which the length of a fiber is fixed while it is wetted and subsequently dried[22] (dotted lines in Figure 3B). Such post-draw fiber processing holds the promise of tailored fiber stiffness. Our model also explains the X-ray diffraction results of Grubb and Jelinski,[24] who differentiated between crystalline, aligned amorphous, and isotropic components in supercontracted fibers.

Such a picture of supercontraction is consistent with previous measurements[6] including NMR experiments probing chain dynamics of various amino acids in supercontracted silk.[14] Our experiments complete this picture by elucidating the role of fiber strain in the process of supercontraction. The major new feature in our interpretation is the incorporation of abrupt strain-dependent transitions between static and mobile phases arising from cooperative reinforcement in local structure by inter- and intrachain hydrogen bonding.

In contrast to as spun dragline silk, viscid silk, found in the capture spiral of the spider web, functions in a microscopically hydrated environment[29] and has mechanical properties similar to supercontracted dragline, suggesting that similar mechanisms are active in these silks. The abundance of proline in the linker regions of viscid silk[30] prevents the formation of stable extended chain structures, which, in addition to a hygroscopic glycoprotein coating,[29] allows viscid silk to maintain its entropic spring character in lower humidity. It has recently been suggested[31] that highly pitched coils act as "nanosprings" in viscid silk. We see no evidence in our data of the existence of such nanosprings in dragline. Instead, our results suggest that latent and mobile entropic springs are responsible for the elastic character of silks.

Acknowledgment. This work was supported by a grant from the Natural Sciences and Engineering Research Council (NSERC) of Canada. P.T.E. thanks NSERC for a post-graduate scholarship. We thank Carolyn Shiau, Bernice Chu, Matt Grinder, and Isaac Leung for help collecting silk samples.

References and Notes

(1) Gosline, J. H.; DeMont, M. E.; Denny, M. W. *Endevour* **1986**, *10*, 36−43.
(2) Vollrath, F.; Knight, D. P. *Nature (London)* **2001**, *410*, 541−548.
(3) Viney, C. In *Structural Biological Materials*; Elices, M., Ed.; Elsevier: Oxford, England, 2000; pp 293−333.
(4) Lazaris, A.; Arcidiacono, S.; Huang, Y.; Zhou, J.-F.; Duguay, F.; Chretien, N.; Welsh, E. A.; Soares, J. W.; Karatzas, C. N. *Science* **2002**, *295*, 472−476.
(5) Guerette, P. A.; Ginzinger, D. G.; Weber, B. H.; Gosline, J. M. *Science* **1996**, *272*, 112−115.
(6) Gosline, J.; Guerette, P.; Ortlepp, C.; Savage, K. *J. Exp. Biol.* **1999**, *202*, 3295−3303.
(7) Liivak, O.; Blye, A.; Shah, N.; Jelinski, L. *Macromolecules* **1998**, *31*, 2947−2951.
(8) Jelinksi, L. W. *Curr. Opin. Solid State Mater. Sci.* **1998**, *3*, 237−245.
(9) Work, R. *Text. Res. J.* **1977**, *47*, 650−662.
(10) Work, R.; Emerson, P. *J. Arachnol.* **1982**, *10*, 1−10.
(11) Bell, F.; McEwen, I.; Viney, C. *Nature (London)* **2002**, *416*, 37.
(12) Guinea, G.; Elices, M.; Perez-Rigueiro, J.; Plaza, G. *Polymer* **2003**, *44*, 5785−5788.
(13) van Beek, J.; Kummerlen, J.; Vollrath, F.; Meier, B. *Int. J. Biol. Macromol.* **1999**, *24*, 173−178.
(14) Yang, Z.; Liivak, O.; Seidel, A.; LaVerde, G.; Zax, D. B.; Jelinski, L. W. *J. Am. Chem. Soc.* **2000**, *122*, 9019−9025.
(15) Parkhe, A.; Seeley, S.; Gardner, K.; Thompson, L.; Lewis, R. *J. Mol. Recognit.* **1997**, *10*, 1−6.
(16) Kummerlen, J.; van Beek, J.; Vollrath, F.; Meier, B. *Macromolecules* **1996**, *29*, 2920−2928.
(17) van Beek, J.; Hess, S.; Vollrath, F.; Meier, B. *Proc. Natl. Acad. Sci. U.S.A.* **2002**, *99*, 10266−10271.
(18) Eles, P. T.; Michal, C. A. *Biomacromolecules*. Submitted July 31, 2003.
(19) Schmidt-Rohr, K.; Hehn, M.; Schaefer, D.; Speiss, H. *J. Chem. Phys.* **1992**, *97*, 2247−2262.
(20) Michal, C.; Broughton, K.; Hansen, E. *Rev. Sci. Instrum.* **2002**, *73*, 453−458.
(21) Dennis, J.; Gay, D.; Welsch, R. *ACM Trans. Math. Software* **1981**, *7*, 348−368.
(22) Perez-Rigueiro, J.; Elices, M.; Guinea, G. *Polymer* **2003**, *44*, 3733−3736.
(23) Shao, Z. Z.; Vollrath, F. *Polymer* **1999**, *40*, 1799−1806.
(24) Grubb, D. T.; Jelinski, L. W. *Macromolecules* **1997**, *30*, 2860−2967.
(25) Simmons, A.; Ray, E.; Jelinski, L. W. *Macromolecules* **1994**, *27*, 5235−5237.
(26) Simmons, A. H.; Michal, C. A.; Jelinski, L. W. *Science* **1996**, *271*, 84−87.
(27) Michal, C. A.; Jelinksi, L. W. *J. Biomol. NMR* **1998**, *12*, 231−241.
(28) Termonia, Y. *Macromolecules* **1994**, *27*, 7378−7381.
(29) Bonthrone, K. M.; Vollrath, F.; Hunter, B. K.; Sanders, J. K. *Proc. R. Soc. London Ser. B* **1992**, *248*, 141−144.
(30) Hayashi, C.; Shipley, N.; Lewis, R. *Int. J. Biol. Macromol.* **1999**, *24*, 271−275.
(31) Becker, N.; Oroudjev, E.; Mutz, S.; Cleveland, J.; Hansma, P.; Hayashi, C.; Makarov, D.; Hansma, H. *Nature Mater.* **2003**, *2*, 278−283.

MA035567P